Journal of Energy Chemistry 41 (2020) 79–86

Contents lists available at ScienceDirect

Journal of Energy Chemistry

journal homepage: www.elsevier.com/locate/jechem

http://www.journals.elsevier.com/journal-of-energy-chemistry/

Role of surface defects of carbon nanotubes on catalytic performance of barium promoted ruthenium catalyst for ammonia synthesis

Yongcheng Ma[a], Guojun Lan[a], Wenzhao Fu[b], Ying Lai[a], Wenfeng Han[a], Haodong Tang[a], Huazhang Liu[a], Ying Li[a,*]

[a] Institute of Industrial Catalysis, Zhejiang University of Technology, Chaowang Road 18, Hangzhou 310014, Zhejiang, China
[b] State Key Laboratory of Chemical Engineering, East China University of Science and Technology, 130 Meilong Road, Shanghai 200237, China

ARTICLE INFO

Article history:
Received 20 February 2019
Revised 6 April 2019
Accepted 12 April 2019
Available online 3 May 2019

Keywords:
Carbon nanotubes
Ruthenium catalyst
Defective carbon
Ammonia synthesis

ABSTRACT

Carbon nanotubes (CNTs) with abundant surface defects are prepared by a liquid oxidation and thermal annealing method. The defective CNTs-D supported Ba–Ru/CNTs-D catalysts exhibit superior catalytic performance in ammonia synthesis with a TOF be increased up to 0.30 s^{-1}, which is 2.5 times of oxidized CNTs-O supported Ba–Ru/CNTs-O catalysts and 5 times of the Ba–Ru/CNTs. The characterizations by CO chemisorption, transmission electron microscope, Raman, and X-ray photoelectron spectroscopy revealed that the uniformly well dispersed Ru NPs can be stabilized on the defective sites of CNTs-D. The great improvement of the catalytic performance and stability of the Ba–Ru/CNTs-D is contributed to the strong interaction between Ru NPs and surface defect of the CNTs.

1. Introduction

Ammonia is not only a vital raw material for chemical fertilizer and valuable chemical, but also a promising energy carrier for storing hydrogen, due to its high capacity for hydrogen storage (17.6 wt%) and facile liquefaction under mild conditions [1,2]. To exploit the use of hydrogen as a source of sustainable energy, development of an efficient process for synthesizing an energy carrier such as ammonia under mild conditions will be necessary. Ruthenium catalysts were recognized as the second-generation catalysts with high activity under mild conditions following conventional iron catalysts [3,4]. The roles of various supports such as activated carbon, CNTs, Al_2O_3, MgO, zeolite and BN [5–11] on the catalytic performance of ammonia synthesis catalyst have been extensively investigated. Carbon materials have been found to be the most effective supports for ammonia synthesis ruthenium catalysts, because they offer unique advantages over traditional metal oxide supports such as extraordinary thermal and electrical conductivity, and tunable surface chemistry and textural properties [12,13].

CNTs supported Ru catalyst has high activity in ammonia synthesis due to its excellent electronic conductivity. However, the surface of pristine CNTs is inert and it is necessary to generate the active sites to anchor the Ru particles [14]. Refluxing the CNTs in boiling nitric acid is one of the most commonly reported methods for introducing a larger number of oxygen-containing surface functional groups (SFGs), which are beneficial for the dispersion of supported metal NPs [15,16]. However, even if it has been demonstrated since many years that oxygen-containing SFGs play a crucial role in carbon supports and can affect dispersion or sintering of the metal particles, it is still a matter of debate whether they also function as anchoring sites for NPs especially for ruthenium based ammonia synthesis catalysts been operated at temperature range of 400–500 °C, at which temperature range, most of the SFGs have already been decomposed [17–19].

Recently, much attention has been focused on the role that surface defects play on some particular performance of carbon materials. Liu et al. and Tao et al. demonstrated that the carbon atoms on the edge defect had a higher electron cloud density than ordinary carbon atoms through density functional theory calculations and their corresponding physical characterization [20,21]. Chen et al. reported defective CNTs supported Pt catalysts in hydrolytic dehydrogenation of ammonia borane and found that defects could stabilize platinum NPs during the reaction [22]. Liu et al. disclosed that Ru NPs deposited on defective graphene exhibits both a high stability against sintering and a superior catalytic performance in hydrogenation reaction [23]. Besides, Zhao et al. presented that the specific topological defects could play a very important role in electro-catalytic oxygen reactions and developed a facile method to create such unique defects [24]. And they employed a simple N-doping and removal method, which will introduce unsaturated

* Corresponding author.
E-mail address: liying@zjut.edu.cn (Y. Li).

https://doi.org/10.1016/j.jechem.2019.04.016

carbon atoms with dangling bonds, thus creating unique defects in the carbon [25]. They also proposed that the used of defective carbons to support metal NPs, and found that the defects can provide stable chemical adsorption sites for metal atoms.

Defective carbon with well-defined metal-defect coordination structures shows good support effect in a series of catalytic reactions, e.g., oxygen reduction reaction [25], hydrogen evolution reaction [26] and hydrolytic dehydrogenation of ammonia borane [22]. However, the study of defective carbon as catalyst support for ammonia synthesis has rarely been reported as far as we known. Herein, we reported a detailed study on the effect of surface defect on catalytic performance in the Ba–Ru/CNTs-D catalyst for ammonia synthesis. Commercialized CNTs (CNTs), oxidized CNTs by HNO_3 (donated as CNTs-O), and defective CNTs (donated as CNTs-D), are employed to immobilize Ru NPs and Ba was used as a promoter for ammonia synthesis.

2. Experimental

2.1. Materials

Commercialized CNTs with surface area of 250 ± 30 m^2/g provided by Nanjing JCNANO Technology Co., LTD were used as a catalyst support. Ruthenium chloride hydrate ($RuCl_3{\cdot}xH_2O$) was purchased from Sino-Platinum Metals Co. Ltd. Other reagents were obtained from Shanghai Chemical Reagent Inc. of Chinese Medicine Group. All materials were of analytical grade and used without any further purification.

2.2. Preparation of the catalysts

(1) Treatment of CNTs: The commercialized CNTs (6 g) was mixed with a solution of 30% HNO_3 (120 mL) at 90 °C for 5 h, then washed until neutral pH value with distilled water, and dried at 120 °C under air overnight (marked with CNTs-O). The CNTs-O was calcined at 850 °C for 10 min in argon (marked with CNTs-D).

(2) Preparation of the Ba–Ru/CNTs: The above pretreated CNTs-*x* (1 g) was first impregnated with a mixed solution of $Ba(NO_3)_2$ (0.076 g) and distilled water (5.6 mL) for 12 h at room temperature, dried at 110 °C for 12 h. Subsequently, the above samples were impregnated with a mixed solution of $RuCl_3{\cdot}xH_2O$ (0.11 g) and distilled water (5.6 mL) for 12 h at room temperature. Then the wet sample was precipitated by diluted ammonia solution (30 vol%) at room temperature for 12 h. After deposition, the samples were washed by deionized water several times at 90 °C until no Cl^- can be detected by $AgNO_3$ solution, and dried at 110 °C for 12 h. The catalysts were reduced under pure H_2 with a flow rate of 30 mL/min at 400 °C for 4 h to obtain reduced Ba–Ru/CNTs-*x* catalysts. The nominal Ba and Ru loading of the catalysts was 3.4 and 3.4 wt%, respectively.

2.3. Measurement of catalytic activities in ammonia synthesis

Ammonia synthesis using the catalyst was carried out in a fixed-bed reactor with an inside diameter of 14 mm at 400–450 °C, space velocity of 10,000 h^{-1}, and 10 MPa. The catalysts (2 mL, 0.90–1.43 mm) were loaded in the isothermal zone of the reactor and activated by a mixture of N_2 and H_2 (N_2:H_2 = 1:3) at a pressure of 5 MPa and a space velocity of 30,000 h^{-1} at 400 °C for 4 h, 425 °C for 8 h, 450 °C for 8 h, and 475 °C for 4 h. After the activation, the temperature was lowered to 400 °C and initial activity was measured. Then the temperature was increased to 475 °C for 12 h with space velocity of 30,000 h^{-1}, and pressure of 5 MPa to test the stability of the catalysts. Under these conditions, the concentration of ammonia in the exit gas of the reactor was measured by sulfuric acid neutralization.

The mass reaction rate of ammonia synthesis was calculated from the following equation [27]:

$$r_m = \frac{S_v V_c}{22.4 W_c} \times \frac{\varphi_{NH_3}}{1+\varphi_{NH_3}}$$

where r_m is mass reaction rate (mmol g^{-1} h^{-1}), W_c is quality of catalyst (g), V_c is volume of catalyst (cm^3), S_v is space velocity of reaction (h^{-1}), and φ_{NH3} is concentration of ammonia in exit gas of reactor (vol%).

2.4. Characterizations

Powder X-ray diffraction (XRD) patterns were recorded on a Rigaku D/Max-2500/pc powder diffraction system using Cu *Kα* radiation (40 kV and 100 mA) over the range $10° \le 2\theta \le 80°$. Nitrogen sorption isotherms were determined at −196 °C by a Quantachrome Autosorb-IQ instrument in the static measurement mode. Before the measurement, the samples were degassed at 300 °C for 10 h.

The Ru content in the catalysts was analyzed by spectrophotometric method with an ultraviolet spectrophotometer (model 7600) from Shanghai Jinghua Instruments Co. Ltd. A typical process is similar to that described in reference [28]: First, 0.10 g catalyst was calcined at 750 °C for 20 min in air to remove carbon support in the catalyst. Second, the residue was mixed with 3.5 g Na_2O_2 under 680 °C for 20 min in a muffle furnace to completely oxidize the Ru^0. The product was then dissolved with a mixed 40 mL concentrated HCl-CH_3CH_2OH solution (volume ratio = 1: 1), and then 10 mL thiourea aqueous solution (0.1 g/mL) was added at 80 °C for 10 min to get a blue, clear solution. Last, the absorbance of as-prepared solution was measured with 620 nm excitation wavelength. The Ru content in the catalyst could be calculated by an external standard method.

The dispersion of Ru was obtained by CO chemisorption method, which was carried out at 40 °C on Quantachrome Autosorb-1/C chemisorb apparatus. Prior to measurements, the pre-reduced catalysts were reduced in situ for 2 h at 400 °C in H_2. The metal dispersion and particle size were estimated based on assumption of a spherical geometry of the particles and an adsorption stoichiometry of one CO molecule on one Ru surface atom.

Transmission electron microscope (TEM) images of the samples were obtained by a FEI Tecnai G20 instrument. The samples were mounted and ultrasonically dispersed in ethanol, and then a few droplets of the suspension were deposited on a copper grid coated by a holey carbon film, followed by drying at ambient conditions.

The X-ray photoelectron spectroscopy (XPS) were recorded on Thermo Scientific Escalab 250Xi equipped with monochromatized Al *Kα* X-ray (1486.6 eV) as the excitation source. Survey spectra were acquired at 40 eV pass energy and the high-resolution spectra were measured at 0.1 eV. The XPS spectra were calibrated by C 1*s* at 284.6 eV.

Hydrogen-temperature-programmed reduction (H_2-TPR) of Ru catalysts was carried out with a self-made TPD/TPR instrument. The mass spectra were collected by an on-line Hiden gas analyzer (QIC 20). Prior to analysis, the samples (cat. 50 mg) were placed in a fixed bed U-shaped quartz tubular reactor located inside an electrical furnace. Then the sample was purged at 110 °C for 1 h in argon stream to remove the adsorbed water and other impurities on the surface of samples. After cooling down to room temperature, the sample was heated to 850 °C at a ramp rate of 10 °C/min under 5% H_2/Ar with a flow rate of 30 mL/min. The following mass signals were monitored simultaneously by a quadrupole mass spectrometer: m/e = 2, 14, 15, 16, 17, 18, 28, 40 and 44 amu.

Acidic-basic titration [29]: NaOH solution with a concentration 0.02 mol/L and HCl solution with a concentration 0.02 mol/L was prepared separately. The CNTs-*x* samples were added to the excess standard NaOH or HCl solutions. Acidic or basic surface functional groups of the carbon surface were determined by back-titration with HCl or NaOH solution after the system reached the equilibrium state.

3. Results and discussion

3.1. Textural properties of the various carbon nanotubes

As reported in the reference [22], the nitric acid liquid oxidation can generate oxidized CNTs (CNTs-O), with SFGs and surface defects on CNTs-O. The removal of oxygen group by the thermal annealing method can create abundant defects (CNTs-D) [30]. The treatment process of the CNTs is shown in Scheme 1. The porosity of pristine CNTs, CNTs-O and CNTs-D was characterized by nitrogen adsorption-desorption method and the corresponding isotherms and pore size distributions are shown in Fig. 1. All the isotherms can be identified as type-IV according to the IUPAC classification and evidenced the mesoporous texture of CNTs. The pore size distributions of CNTs, CNTs-O and CNTs-D based on the BJH method are centered at 46 nm.

Table 1 provides texture properties of the pristine CNTs, oxidized CNTs-O and CNTs-D. The surface areas of all samples were around 250 m^2/g, and the pore volumes were in the range of 2.2–2.7 cm^3/g. From above analysis, the surface area and porosity of the CNTs supports prepared through different treatments does not change. The scanning electron microscope images of CNTs, CNTs-O and CNTs-D samples are given in Fig. S1, indicating that the morphology of CNTs has not changed significantly. The texture properties of various CNTs treated with different methods are almost similar.

Raman and X-ray diffraction techniques were used for characterization of the structure of CNTs, CNTs-O and CNTs-D samples. The XRD patterns of various CNTs are given in Fig. 2(a). There are two peaks at 25.7° and 43.1° for all samples, which are corresponding to the (002) and (101) crystal planes diffraction peaks of graphitic carbon structure. The Raman spectra for these samples are shown in Fig. 2(b), which can be deconvolved into five peaks. Usually, the peaks located at 1340 and 1570 cm^{-1} correspond to defective carbon (D1 band) and graphitic carbon (G band) structures, respectively. While the D2 band at 1620 cm^{-1} is attributed to the presence of disordered structures in CNTs. The D3 band (around 1500 cm^{-1}) has been associated with the amorphous carbon and D4 band (around 1200 cm^{-1}) represents some of the ionic impurities on the carbon surface [31,32]. However, the relative intensity ratio between the D1 band and the G band (I_{D1}/I_G) can be used as an indication of the defect content in the carbon material. The I_{D1}/I_G value for pristine CNTs given in Table 1 is 1.33, and the I_{D1}/I_G value for CNTs-O and CNTs-D is 1.47 and 1.56, respectively, which indicated that CNTs-O and CNTs-D contain more defects than that of CNTs. This is consistent with the results reported in literature [22]. The I_{D1}/I_G value of CNTs-D is higher than that of the CNTs-O, due to the removal of the SFGs causes more defects on CNTs.

Argon temperature-programmed desorption (Ar-TPD) technique was performed to investigate the surface oxygen groups of CNTs, CNTs-O and CNTs-D samples. It has been widely accepted that each type of oxygen-containing SFGs decomposes to a defined product. For example, CO_2 generates from the decomposition of carboxylic acids at low temperatures (127–527 °C) or from lactones at high temperatures (427–827 °C); carboxylic anhydrides (327–627 °C) and pyrones (above 1097 °C) originate both CO and CO_2; groups such as phenols (527–927 °C), carbonyls (800–900 °C) and quinones (427–627 °C) originate CO [5,33,34]. The CO_2 desorption profiles of various samples are shown in Fig. 3(a), the amount of CO_2 increases dramatically after nitric acid treatment, suggesting that the CNTs-O contain relatively more carboxyl and lactones groups. The least amounts of CO_2 were released from CNTs and CNTs-D, indicating that they have a small amount of oxygen functional groups. From Fig. 3(b), CO begins to desorb at about 400 °C for CNTs-O sample, and the amount of desorption is significantly increased, further indicating that the CNTs-O may have phenols, ethers, carbonyls and quinones groups [35]. However, there are two CO peaks at 627 and 770 °C for pristine CNTs, which can be assigned to quinones and phenols groups; this could be the residual oxygen species in the preparation of carbon nanotubes. And only one sharp desorption peak of CO at approximately 800 °C for CNTs-D sample, which can be assigned to the carbonyls groups [29,31], showing that after thermal annealing of CNTs-O, most of the SFGs have been removed. The above results were further confirmed from the results of chemical titration (Table 1) that most of the acidic functional groups can be generated by the nitric acid treatment. However, the results of Boehm titration also showed that CNTs-D had the highest basic functional groups content, which also indicated that carbonyls groups were produced after the thermal annealing treatment at 850 °C [29]. Thus, the gradual detachment of the oxygen functional groups during the annealing causes the formation of dangling bonds on carbon atoms, resulting in the formation of defective carbon [30].

3.2. Textural properties of Ba-Ru/CNTs-x catalysts

The N_2 adsorption-desorption isotherms and pore size distribution of various Ba–Ru/CNTs-*x* catalysts are given in Fig. S2. Table 2 lists the specific surface area, total pore volume and the average pore diameter of the Ba–Ru/CNTs-*x* catalysts. The textural properties of Ba–Ru/CNTs-*x* catalysts are almost unchanged, which indicates that the supporting of the active components has no effect on the texture properties of CNTs due to its high surface area and large pore diameter.

To study the status and size of Ru NPs, X-ray diffraction, transmission electron microscopy and CO chemisorption characterization were carried out. The XRD patterns of all Ba–Ru/CNTs-*x* catalysts are shown in Fig. S3. There are only two peaks at 25.7° and 43.1° assigned to the (002) and (101) diffraction peaks of graphitic carbon for all catalysts. No distinct ruthenium metal or other ruthenium compound reflections were visible, which showed evidence that Ru NPs were well dispersed on these catalysts. Fig. 4 shows typical TEM images and corresponding particle size distributions of the Ba–Ru/CNTs-*x* catalysts. The Ba–Ru/CNTs-O and Ba–Ru/CNTs-D catalysts have well dispersed Ru NPs with narrow particle size distributions in the range of 1.5–2.5 nm, and

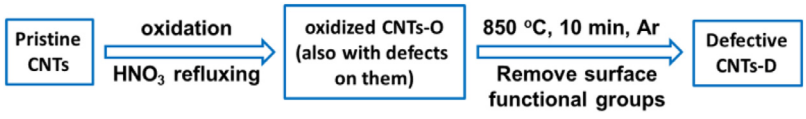

Scheme 1. Pretreatment of CNTs to obtain CNTs-D.

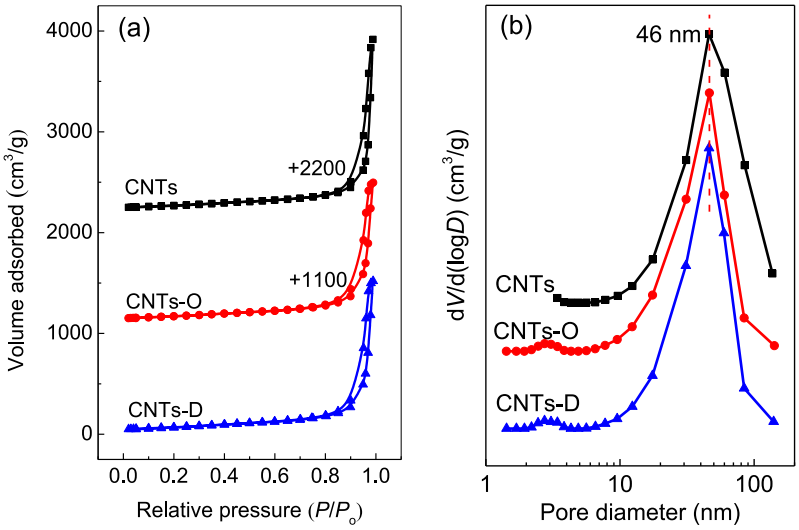

Fig. 1. (a) Nitrogen adsorption–desorption isotherms and (b) pore size distribution of the CNTs, CNTs-O and CNTs-D.

Table 1. Texture properties and concentration of surface functional groups of CNTs, CNTs-O and CNTs-D.

Samples	S. A. (m^2/g)	P. V. (cm^3/g)	P. D.[a] (nm)	I_{D1}/I_G	Acidic functional groups (mmol/g)	Basic functional groups (mmol/g)
CNTs	251	2.7	46	1.33	0.03	0.03
CNTs-O	252	2.2	46	1.47	0.23	0.01
CNTs-D	248	2.4	46	1.56	0.02	0.08

S.A.: Surface area; P.V.: Pore volume; P.D.: Pore diameter.
[a] Using the BJH desorption data.

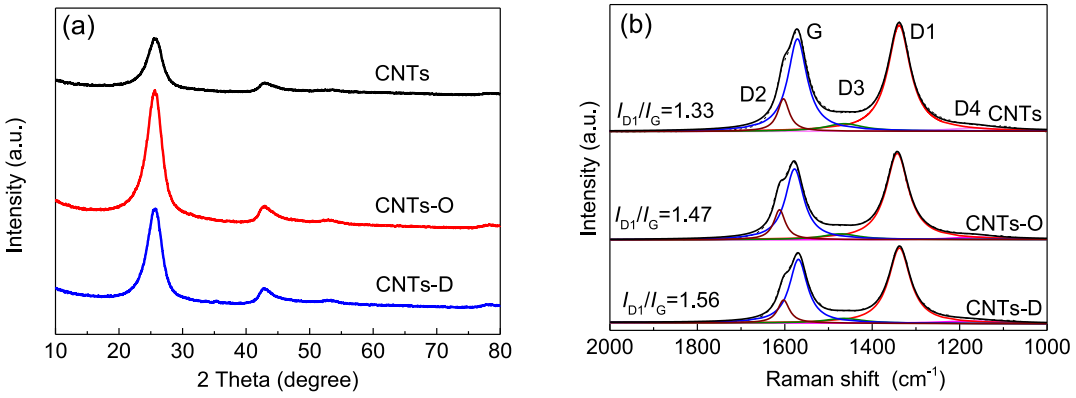

Fig. 2. (a) XRD patterns and (b) Raman spectra of CNTs, CNTs-O and CNTs-D supports.

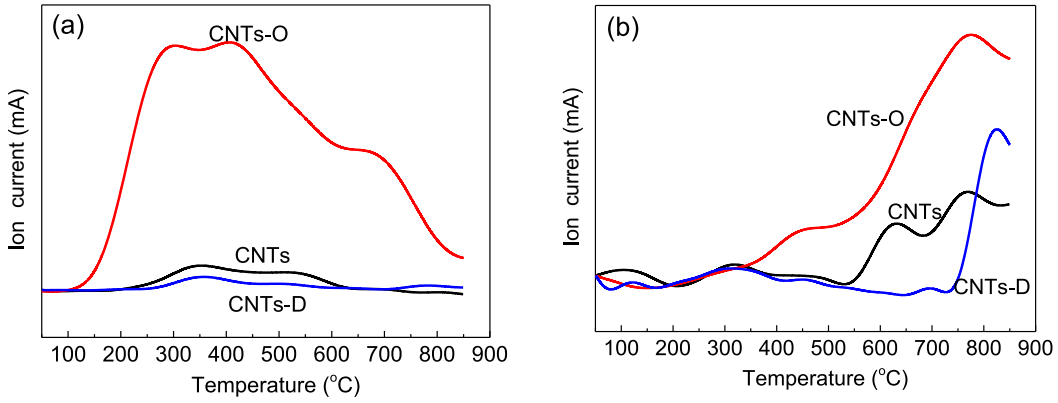

Fig. 3. Ar-TPD-MS profiles of CNTs, CNTs-O and CNTs-D. (a) CO_2 evolution ($m/e = 44$); (b) CO evolution ($m/e = 28$).

Table 2. Texture properties and dispersion of Ba–Ru/CNTs-*x* catalysts.

Catalysts	S. A. (m^2/g)	P. V. (cm^3/g)	P. D.[a] (nm)	Ru[b] (%)	CO chemisorption			TEM		TOF[d] (s^{-1})
					CO uptake (μmol/g)	Dispersion (%)	Ru particle size (nm)	Dispersion[c] (%)	Ru particle size (nm)	
Ba–Ru/CNTs	214	1.7	46	2.85	92.1	32.8	4.1	49.3	2.7	0.07
Ba–Ru/CNTs-O	276	1.9	46	2.90	123.2	43.2	3.1	63.3	2.1	0.12
Ba–Ru/CNTs-D	260	2.2	46	2.94	102.0	35.3	3.8	57.8	2.3	0.30

S.A.: Surface area; P.V.: Pore volume; P.D.: Pore diameter.
[a] Using the BJH desorption data.
[b] Ru loadings was measured by the spectrophotometric method.
[c] Ru dispersion was obtained by using the equation $D_{Ru} = 1.33/d_{Ru}$.
[d] TOF was calculated from the rate of ammonia synthesis at 450 °C divided by CO uptake.

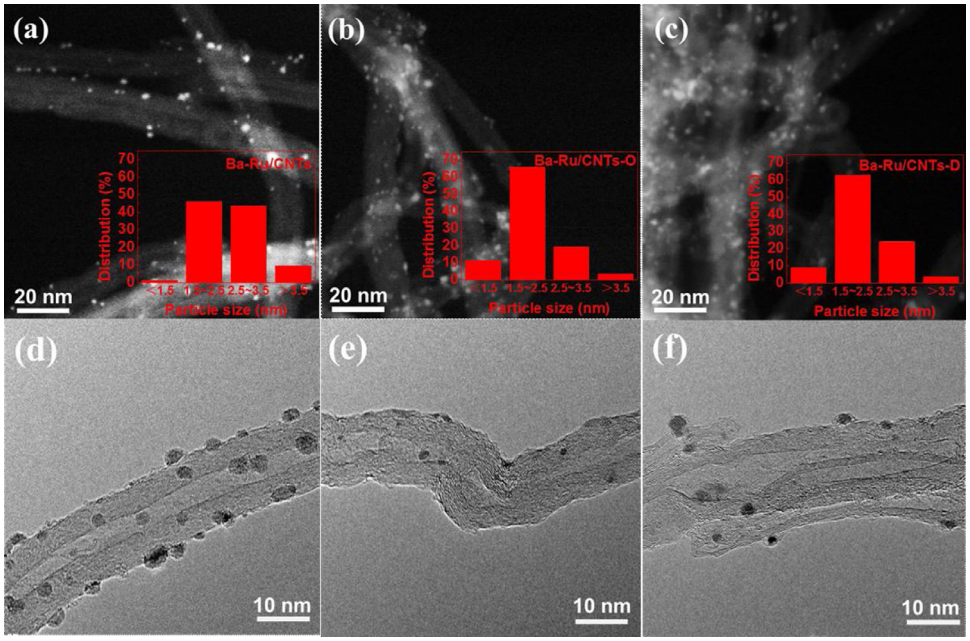

Fig. 4. Representative TEM images and corresponding particle size distributions for Ru catalysts: (a, d) Ba–Ru/CNTs, (b, e) Ba–Ru/CNTs-O and (c, f) Ba–Ru/CNTs-D.

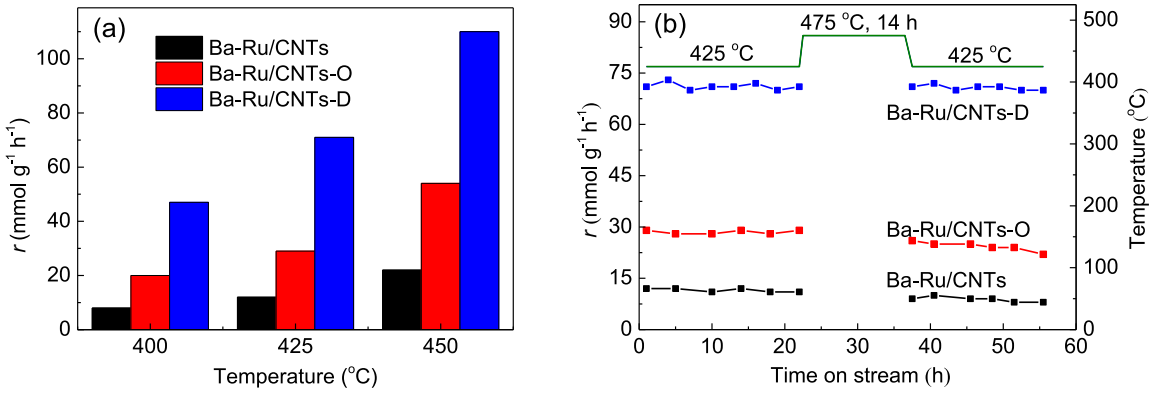

Fig. 5. (a) Ammonia synthesis rates of Ba–Ru/CNTs, Ba–Ru/CNTs-O and Ba–Ru/CNTs-D catalysts at various temperatures; (b) The reaction rate of Ba–Ru/CNTs, Ba–Ru/CNTs-O and Ba–Ru/CNTs-D catalysts as a function of time on stream in ammonia synthesis before and after thermal resistance test (Reaction conditions: 425 °C, 10 MPa, $H_2/N_2 = 3/1$, 10,000/h).

Table 3. Relative abundance (%) of the components of the Ru 3*p* spectra.

Catalysts	Peak 1		Peak 2		Peak 3	
	BE (eV)	Area (%)	BE (eV)	Area (%)	BE (eV)	Area (%)
Ru/CNTs	462.9	63.0	465.7	37.0	–	–
Ru/CNTs-O	462.9	79.7	465.7	20.3	–	–
Ru/CNTs-D	462.8	85.0	465.6	15.0	–	–
Ba–Ru/CNTs	462.7	32.0	465.5	37.0	467.9	31.0
Ba–Ru/CNTs-O	462.7	52.8	465.5	37.9	467.9	9.3
Ba–Ru/CNTs-D	462.6	56.3	465.4	43.7	–	–

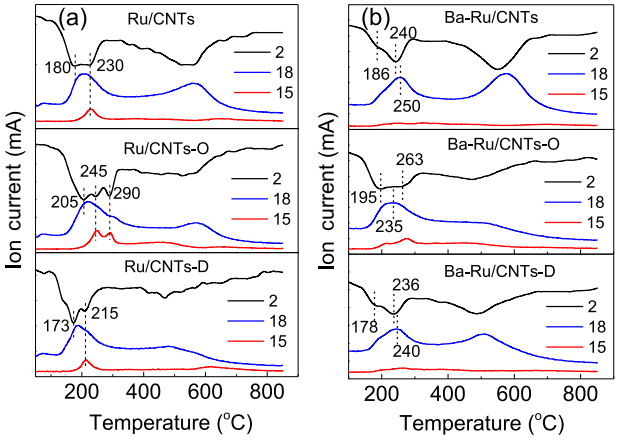

Fig. 6. Temperature-programmed reduction profiles of the Ru/CNTs-*x* (a) and Ba–Ru/CNTs-*x* (b) under 5% H_2/Ar atmosphere detected with a mass spectrometer.

no big particle aggregation is observed. The average Ru NPs for Ba–Ru/CNTs is 2.7 nm, which is larger than the Ba–Ru/CNTs-O and Ba–Ru/CNTs-D, which are 2.1 and 2.3 nm, respectively.

The dispersion and particle size of Ru NPs determined by CO chemisorption and compared with that obtained by TEM are given in Table 2. Based on the chemisorption data and assuming an adsorption stoichiometry of one molecule of CO molecule on one metal surface atom, one can estimate the dispersion of the metal catalysts [36]. The level of CO chemisorption is 92.1, 123.2 and 102.0 μmol/g for Ba–Ru/CNTs, Ba–Ru/CNTs-O and Ba–Ru/CNTs-D catalysts, respectively. The increase of the SFGs can increase the dispersion of the Ru NPs as evidenced by the increasing amount of CO adsorption for Ba–Ru/CNTs-O compared with the pristine CNTs supported Ba–Ru/CNTs catalyst. This result is the same with our previous reports on the activated carbon supported ruthenium catalysts [37]. The amount of CO adsorption for Ba–Ru/CNTs-D is also increased compared with the Ba–Ru/CNTs although they have similar oxygen content. The surface structure of CNTs support changed after the CNTs been oxidized and thermal treated. This further indicates the defects can disperse the Ru NPs well. But the CO adsorption of Ba–Ru/CNTs-D is decreased compared with that of the Ba–Ru/CNTs-O. The average sizes of Ru particles obtained from CO chemisorption for Ru catalysts were higher than those based on TEM. The presence of residual chlorine or carbon may lead to the blockage of the Ru sites for CO adsorption [38]. Therefore, the size of Ru particles based on CO chemisorption would be overestimated. However, the trend of the various catalysts is similar although the accuracy of the dispersion is affected by the CO adsorption method.

3.3. Catalytic performance of Ba–Ru/CNTs-x catalysts in ammonia synthesis

Fig. 5(a) displays the catalytic performance of Ba–Ru/CNTs-*x* catalysts for ammonia synthesis rates at different temperatures at 10 MPa, 10,000 h^{-1} and $H_2/N_2 = 3.0$. The activities of Ru catalysts increase with the increasing of the reaction temperatures in the range of 400–450 °C. At the temperature range studied, the activity increased in the order of Ba–Ru/CNTs < Ba–Ru/CNTs-O < Ba–Ru/CNTs-D. The increasing catalytic performance of the oxidized CNTs-O supported catalysts is reasonable according to the results in our previous reports and references [5,15] due to the increasing of SFGs can increase the dispersion of Ru NPs. It is interesting to note that the catalytic performance of Ba–Ru/CNTs-D shows the highest ammonia synthesis rate at 450 °C (110 mmol g^{-1} h^{-1}) although the dispersion of Ru NPs is lower than that of the Ba–Ru/CNTs-O catalysts. The turnover frequency (TOF) data was calculated based on the CO adsorption data, which is given in Table 2. The TOF value for Ba–Ru/CNTs, Ba–Ru/CNTs-O, and Ba–Ru/CNTs-D is 0.07, 0.12, and 0.30/s, respectively. The TOF value for defective CNTs-D supported catalysts is 2.5 times higher than that for the oxidized CNTs-O supported catalysts. The Ru NPs size effects are exclude considering the fact that the size of Ru NPs size in Ba–Ru/CNTs-O and Ba–Ru/CNTs-D catalysts are essentially similar. Therefore, the difference rate of ammonia synthesis in above catalysts may be related to the electronic state of Ru NPs and the interaction between Ru and carbon support.

Since the treatment of the catalysts under severe condition is helpful for estimating the stability of carbon-supported Ru catalysts, a high temperature treatment process at 475 °C for 14 h was carried out. Most of unstable catalysts resulted in a decreasing performance after the severer thermal treatments [39,40]. To evaluate the stability of the catalysts, Fig. 5(b) shows the ammonia synthesis rates as a function of time on stream. The reaction rate of Ba–Ru/CNTs-D remains unchanged after 14 h thermal treatments, while the Ba–Ru/CNTs-O and Ba–Ru/CNTs are reduced to different extents. This means that the carbon structure affects the thermal stability of the catalysts. Furthermore, the used Ba–Ru/CNTs, Ba–Ru/CNTs-O and Ba–Ru/CNTs-D catalysts were characterized by CO chemisorption. Table S1 gives the dispersion and particle size of Ru NPs in various Ru catalysts after the reaction. Results in Table S1 reveal that the CO uptake of Ba–Ru/CNTs-D decreased from 102.0 to 75.8 μmol/g after been used, meaning a 25.7% loss in the CO uptake; while the CO uptake loss rates for the Ba–Ru/CNTs and Ba–Ru/CNTs-O catalysts were 31.3% and 42.5%, respectively, indicating

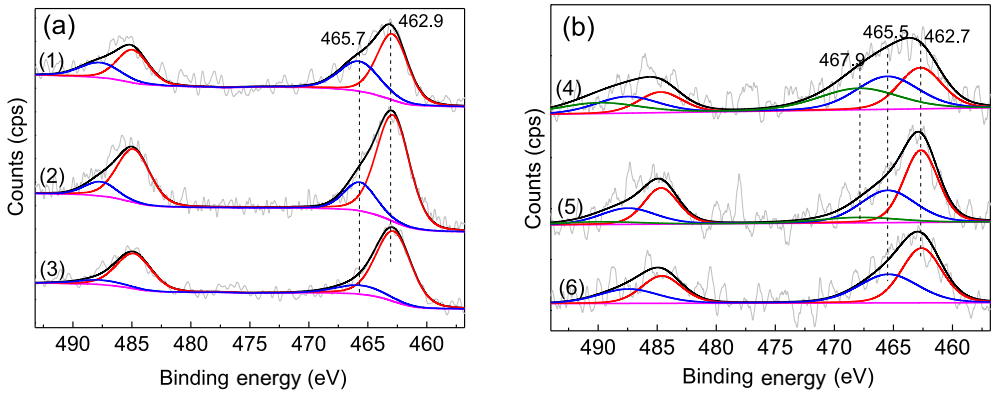

Fig. 7. X-ray photoelectron spectroscopy spectra of Ru 3*p* for various (a) Ru/CNTs-*x* and (b) Ba–Ru/CNTs-*x* catalysts. (1) Ru/CNTs; (2) Ru/CNTs-O; (3) Ru/CNTs-D; (4) Ba–Ru/CNTs; (5) Ba–Ru/CNTs-O; (6) Ba–Ru/CNTs-D.

that the defect-rich CNTs-D can stabilize the Ru NPs, and the Ba-Ru/CNTs-D has the highest dispersion in the Ru catalysts after the reaction.

3.4. Status of Ru species on various CNTs-x support

To further identify the interaction between Ru NPs and the carbon framework, a series of hydrogen temperature-programmed reduction of the various catalysts were performed under 5% H_2/Ar and the signal of H_2, H_2O, CH_4, CO and CO_2 were detected with a mass spectrometer. For clarity, both the Ru/CNTs-*x* and Ba–Ru/CNTs-*x* are characterized. The H_2-TPR patterns of Ru/CNTs-*x* without barium promoters are shown in Fig. 6(a) and the Ba–Ru/CNTs-*x* are shown in Fig. 6(b). The information of the TPR peaks is summarized in Table S2. The first peak appears at 180 °C, 205 °C and 173 °C for Ru/CNTs, Ru/CNTs-O, and Ru/CNTs-D, respectively, which can be assigned to the reduction of RuO_x since only the H_2O signal appeared at corresponding temperature ranges. As reported in the experimental part, all the catalysts were prepared by diluted ammonia solution assisted precipitation method. The $RuCl_3$ has been precipitated into $Ru(OH)_3$ by ammonia and the ruthenium hydroxide can be decomposed into ruthenium oxide during dry process. This has been fully discussed in our previous reports [5]. The second peaks at 215–290 °C, can be assigned to the methanation of carbon support with H_2; there are corresponding CH_4 signals are detected with consumption of H_2 signals. As is known, existence of Ru metal can catalyze the methanation of carbon support under hydrogen atmosphere.

From the above results, both the RuO_x reduction and carbon methanation peaks are shifted into higher temperature for Ru/CNTs-O compared with the Ru/CNTs, while the reduction peaks are shifted to lower temperature for Ru/CNTs-D compared with that of the Ru/CNTs. This observation can be explained by an easier methanation of the Ru/CNTs-D samples than for other two samples owing to the strong interaction between Ru NPs and the carbon support [36]. The last peaks of Ru/CNTs, Ru/CNTs-O and Ru/CNTs-D samples are higher than 470 °C, which can be considered as the decomposition of oxygen-containing groups on the surface of the samples [39]; both water, CO and CO_2 molecules are detected by a mass spectrometer in this temperature range. See supporting information Fig. S4. Fig. 6(b) shows H_2-TPR profiles of the Ba–Ru/CNTs-*x* catalysts. The trend of Ba–Ru/CNTs-*x* catalysts curve is like that of Ru/CNTs-*x* samples. A new peak at ca. 240 °C appears for all the samples accompanied with a H_2O signal at same range. But these peaks appear at similar range with that of the RuO_x reduction. It is difficult to separate them. According to the preparation process, $Ba(OH)_2$ maybe formed after precipitation by ammonia solution [41]. Therefore, only the H_2O signals are detected at this temperature range.

The electron structure of Ru NPs in catalysts is very important due to the dissociation of N_2 is the rate-determining step in ammonia synthesis. The enhancement of the catalytic activity is ascribed to the transfer of electrons from Ru to the anti π orbital of N_2 [42]. From above discussion, Ba–Ru/CNTs-O and Ba–Ru/CNTs-D catalysts have similar Ru NPs particles size, but their TOFs values are different. Therefore, XPS technique was adopted to characterize the electron status of the Ru catalysts. Due to the overlapping of the Ru $3d_{3/2}$ peak with the C 1*s* peak (284.6 eV), the binding energy of the Ru 3*p* peak was used to determine the states of Ru present on the surface [43]. To identify the role of CNTs supports clearly, the Ru/CNTs-*x* was tested together with Ba–Ru/CNTs-*x* samples.

Fig. 7(a) illustrates the Ru 3*p* XPS results of the Ru/CNTs-*x* samples; the Ru peaks are fitted into two peaks with binding energy of ca. 462.9 and 465.7 eV, which can be assigned to Ru^0 (i.e., metallic Ru) and Ru^{n+} (i.e., RuO_x), respectively [4,44]. The deconvolution results including the binding energy and relative content of different peaks are shown in Table 3. It should be noted that the Ru 3*p* XPS peaks for pure metallic Ru are around 461.5 eV [43], while for carbon supported Ru catalysts, the binding energy is higher than that of metallic Ru in elementary substance, indicating that Ru is electron deficient for all carbon materials due to the difference in electronegativity between Ru and C or O [45,46]. The relative content of Ru^0 (85.0%) in Ru/CNTs-D is higher than those of Ru/CNTs and Ru/CNTs-O samples. This indicated that the defective CNTs-D has stronger interaction with the Ru NPs and reduces the electron transfer from Ru to CNTs-D. As a result, the binding energy is relatively lower than those of Ru/CNTs and Ru/CNTs-O samples [47]. This is confirmed by the easier reduction behavior of the Ru/CNTs-D than that of the Ru/CNTs as demonstrated by the results of H_2-TPR. Fig. 7(b) shows Ru 3*p* XPS results of the Ba-Ru/CNTs-*x* catalysts and the fitting results and analysis data are provided in Table 3.

The addition barium promoter to the Ru/CNTs-*x* series causes the binding energy of the Ru 3*p* peaks shift to lower energy for all the Ba–Ru/CNTs-*x* samples. And the ratio of cationic ruthenium species is increased for Ba–Ru/CNTs and Ba–Ru/CNTs-O samples. A third peaks was fitted to get a better fitting curves, which indicates that the barium greatly affected the electronic status of Ba–Ru/CNTs catalysts. This is reasonable since the barium are considered to remain in metal oxide status on the promoted catalysts. For Ba–Ru/CNTs-D catalyst, there are still two species for Ru^0 and Ru^{n+} can be fitted properly. This could be due to that the defects on the CNTs-D can increase the metallic status of ruthenium.

From the above characterizations, the structure of ruthenium particles is greatly affected by the surface structure of CNTs; to further identify the effect of the carbon supports on catalytic performance of the catalysts, the activation energies for Ba–Ru/CNTs, Ba–Ru/CNTs-O and Ba–Ru/CNTs-D are calculated based the reaction rate at different temperatures, which are 81.6, 80.1 and 68.8 kJ/mol, respectively. The activation energy for Ba–Ru/CNTs-D in ammonia synthesis is the lowest among all the catalysts, indicates that the defective CNTs-D supported catalysts are highly active in ammonia synthesis than other two catalysts. The high catalytic performance can be attributed to the strong metallic state of Ru NPs and the interaction between Ru and carbon support for Ba–Ru/CNTs-D. Liu et al. [48] performed first-principles calculations and showed that the stability of a Ru_{13} particle is enhanced on the defective graphene substrate due to the hybridization between the Ru_{13} particles with the sp^2 dangling bonds at the defect sites. And the local curvature formed at the interface will also increase the diffusion barrier of the Ru atom, prohibiting the particle sintering, thereby improving the stability of the reaction. Machado et al. [17] calculated by DFT that the binds ability of Ru_{13} cluster to graphene double vacancies is stronger than that of original graphene, which enhance the interaction between metal NPs and carbon support, and makes Ru NPs have higher thermal stability. As discussed above, the defects on CNTs-D improve the metallic properties of the Ru and the thermal stability of the Ru NPs, thereby reducing the apparent activation energy and increasing the TOF value of the ammonia synthesis reaction.

4. Conclusions

In summary, it is a facile and effective method to introduce defective sites on CNTs by acid oxidation and subsequent high temperature treatments. Such defect-rich CNTs-D support immobilized Ru NPs and Ba promotes catalyst has the highest activity compare to the Ru NPs supported on oxidization CNTs-O and pristine CNTs. The strong interaction between surface defect and Ru NPs greatly improves the catalytic performance and stability of ammonia syn-

thesis. The present work indicates that the carbon defects play key roles in Ba–Ru/CNTs-D catalysts for ammonia synthesis.

Acknowledgments

The financial support from Natural Science Foundation of Zhejiang Province (LY17B030010) is gratefully acknowledged.

Supplementary material

Supplementary material associated with this article can be found, in the online version, at doi:10.1016/j.jechem.2019.04.016.

References

[1] J.P. Guo, P. Chen, Chem 3 (2017) 709–712.
[2] Q.R. Wang, J.P. Guo, P. Chen, J. Energy Chem. 36 (2019) 25–36.
[3] H.Z. Liu, Chin. J. Catal. 35 (2014) 1619–1640.
[4] W.F. Han, L.H. Li, H.Y. Yan, H.D. Tang, Z. Li, Y. Li, H.Z. Liu, ACS Sustain. Chem. Eng. 5 (2017) 7195–7202.
[5] Y. Li, C.G. Pan, W.F. Han, H.F. Chai, H.Z. Liu, Catal. Today 174 (2011) 97–105.
[6] S.J. Guo, X.L. Pan, H.L. Gao, Z.Q. Yang, J.J. Zhao, X.H. Bao, Chem. Eur. J. 16 (2010) 5379–5384.
[7] W.B. Gao, P.K. Wang, J.P. Guo, F. Chang, T. He, Q.R. Wang, G.T. Wu, P. Chen, ACS Catal. 7 (2017) 3654–3661.
[8] B.Y. Lin, R. Wang, J.X. Lin, J. Ni, K.M. Wei, Catal. Commun. 12 (2011) 553–558.
[9] C. Huo, Q.H. Xia, Y. Luo, X.Z. Yang, H.Z. Liu, Chin. J. Catal. 30 (2009) 537–542.
[10] M.D. Cisneros, J.H. Lunsford, J. Catal. 141 (1993) 191–205.
[11] C.F. Xu, Y.L. Ou, J. Zhang, B. Zhou, Y. Li, H.Z. Liu, Chin. J. Catal. 31 (2010) 677–682.
[12] X.L. Zheng, S.J. Zhang, J.X. Xu, K.M. Wei, Carbon 40 (2002) 2597–2603.
[13] W. Jiang, Y. Li, W.F. Han, Y.P. Zhou, H.D. Tang, H.Z. Liu, J. Energy Chem. 23 (2014) 443–452.
[14] J.L. Chen, Z.H. Zhu, S.B. Wang, Q. Ma, V. Rudolph, G.Q. Lu, Chem. Eng. J. 156 (2010) 404–410.
[15] W.F. Han, H.Z. Liu, H. Zhu, Catal. Commun. 8 (2007) 351–354.
[16] B.Y. Lin, Y.J. Guo, C.F. Cao, J. Ni, J.X. Lin, L.L. Jiang, Catal. Today 316 (2018) 230–236.
[17] B.F. Machado, M. Oubenali, M.R. Axet, T.T. Nguyen, M. Tunckol, M. Girleanu, O. Ersen, I.C. Gerber, P. Serp, J. Catal. 309 (2014) 185–198.
[18] W.Y. Chen, J. Ji, X.Z. Duan, G. Qian, P. Li, X.G. Zhou, D. Chen, W.K. Yuan, Chem. Commun. 50 (2014) 2142–2144.
[19] Y. Wang, Z.M. Rong, Y. Wang, J.P. Qu, J. Catal. 333 (2016) 8–16.
[20] D.D. Liu, L. Tao, D.F. Yan, Y.Q. Zou, S.Y. Wang, ChemElectroChem 5 (2018) 1775–1785.
[21] L. Tao, M. Qiao, R. Jin, Y. Li, Z.H. Xiao, Y.Q. Wang, N.N. Zhang, C. Xie, Q.G. He, D.C. Jiang, G. Yu, Y.F. Li, S.Y. Wang, Angew. Chem. Int. Ed. 58 (2019) 1019–1024.
[22] W.Y. Chen, X.Z. Duan, G. Qian, D. Chen, X.G. Zhou, ChemSusChem 8 (2015) 2927–2931.
[23] X. Liu, K.X. Yao, C.G. Meng, Y. Han, Dalton Trans. 41 (2012) 1289–1296.
[24] H.Y. Zhao, C.H. Sun, Z. Jin, D.W. Wang, X.C. Yan, Z.G. Chen, G.S. Zhu, X.D. Yao, J. Mater. Chem. A 3 (2015) 11736–11739.
[25] X.C. Yan, Y. Jia, T. Odedairo, X.J. Zhao, Z. Jin, Z.H. Zhu, X.D. Yao, Chem. Commun. 52 (2016) 8156–8159.
[26] J. Liu, Y.Y. Yue, H.Y. Liu, Z.J. Da, C.C. Liu, A.Z. Ma, J.F. Rong, D.S. Su, X.J. Bao, H.D. Zheng, ACS Catal. 7 (2017) 3349–3355.
[27] Y.P. Zhou, G.J. Lan, B. Zhou, W. Jiang, W.F. Han, H.Z. Liu, Y. Li, Chin. J. Catal. 34 (2013) 1395–1401.
[28] X.Y. Liu, G.J. Lan, P.P. Su, L.H. Qian, T.R. Reina, L. Wang, Y. Li, J. Liu, Catal. Today (2018), doi:10.1016/j.cattod.2018.12.039.
[29] H.P. Boehm, Carbon 40 (2002) 145–149.
[30] Y.Y. Qiu, S. Ali, G.J. Lan, H.Q. Tong, J.T. Fan, H.Y. Liu, B. Li, W.F. Han, H.D. Tang, H.Z. Liu, Y. Li, Carbon 146 (2019) 406–412.
[31] Y.J. Zhang, J. Wang, J.F. Rong, J.Y. Diao, J.Y. Zhang, C.F. Shi, H.Y. Liu, D.S. Su, ChemSusChem 10 (2017) 353–358.
[32] M. Knauer, M.E. Schuster, D.S. Su, R. Schlogl, R. Niessner, N.P. Ivleva, J. Phys. Chem. A 113 (2009) 13871–13880.
[33] J.L. Figueiredo, M.F.R. Pereira, M.M.A. Freitas, J.J.M. Órfão, Carbon 37 (1999) 1379–1389.
[34] G.J. Lan, Y.Y. Qiu, J.T. Fan, X.L. Wang, H.D. Tang, W.F. Han, H.Z. Liu, H.Y. Liu, S. Song, Y. Li, Chem. Commun. 55 (2019) 1430–1433.
[35] J.L. Figueiredo, M.F.R. Pereira, Catal. Today 150 (2010) 2–7.
[36] G.J. Lan, H.D. Tang, Y.P. Zhou, W.F. Han, H.Z. Liu, X.N. Li, Y. Li, ChemCatChem 6 (2014) 353–360.
[37] Y. Li, G.J. Lan, G.Q. Feng, W. Jiang, W.F. Han, H.D. Tang, H.Z. Liu, ChemCatChem 6 (2014) 572–579.
[38] B.Y. Lin, K.M. Wei, J. Ni, J.X. Lin, ChemCatChem 5 (2013) 1941–1947.
[39] B.Y. Lin, Y.C. Qi, Y.J. Guo, J.X. Lin, J. Ni, Catal. Sci. Technol. 5 (2015) 2829–2838.
[40] B.Y. Lin, Y.J. Guo, J.D. Lin, J. Ni, J.X. Lin, L.L. Jiang, Y. Wang, Appl. Catal. A-Gen. 541 (2017) 1–7.
[41] H.S. Zeng, K. Inazu, K-I. Aika, Appl. Catal. A-Gen. 219 (2001) 235–247.
[42] C.N.R. Rao, G.R. Rao, Surf. Sci. Rep. 13 (1991) 221–263.
[43] J.Y. Shen, A. Adnotm, S. Kaliaguine, Appl. Surf. Sci. 51 (1991) 47–60.
[44] J. Li, Y. Liang, Q. Liao, X. Zhu, X. Tian, Electrochim. Acta 54 (2009) 1277–1285.
[45] Y. Wang, Z.M. Rong, Y. Wang, P. Zhang, Y. Wang, J.P. Qu, J. Catal. 329 (2015) 95–106.
[46] W.J. Gao, S.J. Guo, H.B. Zhang, X.L. Pan, X.H. Bao, Chin. J. Catal. 32 (2014) 1418–1423.
[47] X.Y. Sun, R. Wang, B.S. Zhang, R. Huang, X. Huang, D.S. Su, T. Chen, C.X. Miao, W.M. Yang, ChemCatChem 6 (2014) 2270–2275.
[48] X. Liu, C.G. Meng, Y. Han, Nanoscale 4 (2012) 2288–2295.